A Recursive Approach to Space Resection Using Straight Lines

Antonio Maria Garcia Tommaselli and Clésio Luis Tozzi

Abstract

An approach using straight lines as features to solve the photogrammetric space resection problem is presented. An explicit mathematical model relating straight lines, in both object and image space, is used. Based on this model, Kalman Filtering is applied to solve the space resection problem. The recursive property of the filter is used in an iterative process which uses the sequentially estimated camera location parameters to feedback to the feature extraction process in the image.

This feedback process leads to a gradual reduction of the image space for feature searching, and consequently eliminates the bottleneck due to the high computational cost of the image segmentation phase. It also enables feature extraction and the determination of feature correspondence in image and object space in an automatic way, i.e., without operator interference.

Results obtained from simulated and real data show that highly accurate space resection parameters are obtained as well as a progressive processing time reduction.

The obtained accuracy, the automatic correspondence process, and the short related processing time show that the proposed approach can be used in many real-time machine vision systems, making possible the implementation of applications not feasible until now.

Introduction

Space resection problems are not restricted to photogrammetric applications; they are also found in machine vision systems. Specifically in robotics, a machine vision system can be implemented using a camera positioned either remotely (eye-off-hand) or attached to the robot wrist (eye-in-hand). In the eye-in-hand system, the key problem is the determination of the camera location and orientation, relative to the global or object reference system, each time a movement is made. In the eye-off-hand configuration, on the other hand, camera location and orientation are known, and tracking or determination of the wrist position becomes the problem. In both cases, the solution is obtained using a space resection approach.

To solve the space resection problem, the six unknown parameters (three rotations and three translations) are computed using a set of control points whose coordinates are known both in the image and in the world reference systems. In spite of its wide dissemination, the classical method presents two fundamental problems in real-time applications: (1) The solution of a system of non-linear equations and (2) automatic feature extraction and correspondence.

The solution of a system of non-linear equations requires linearizations, and an iterative procedure must be used which is time consuming and, thus, improper for real-time applications. Solutions which attempt to reduce the computational costs related to the linearization process have been proposed in the literature (see, for example, Lenz and Tsai (1988) and Fischler and Bolles (1981)).

Automatic feature extraction and correspondence is of crucial importance in real-time applications, given that point determination in the image and its correspondence to the control points in object space must be conducted in an automatic way, i.e., without operator interference. This requires the use of image segmentation techniques which are time consuming and may become a bottleneck in the whole process, because the computational cost of feature extraction is much higher than is the cost of parameter estimation. Lee *et al.* (1990) reported an experiment using a rectangular shape based model. In their approach, the image processing steps required 32 seconds while the solution to the space resection equations used only 1.07 ms in a Sun workstation. Similar considerations regarding this bottleneck are presented by Gruen (1992).

Another approach that tries to overcome these problems is the use of more meaningful features, such as straight lines, curved lines, rectangular shapes, junctions, etc., instead of points. Among these features, straight lines have been largely preferred because they present some advantages over other features:

- Identification of straight lines in the image is easier than the identification of points, and the correspondence problem can be solved with a smaller probability of gross errors;
- Straight line parameters can be obtained with subpixel precision; and
- There are many straight lines in images of industrial environments.

The use of alternative features in the space resection problem has recently received increasing attention, and some methods have been proposed in the literature (Lugnani, 1980; Tommaselli and Lugnani, 1988; Mulawa and Mikhail, 1988; Dhome *et al.*, 1989; Chen *et al.*, 1989; Salari and Jong, 1990; Liu *et al.*, 1990; Wang and Tsai, 1990; Lee *et al.*, 1990; Echigo, 1990; Chen and Jiang, 1991; Chen and Tsai, 1991).

For some applications, even the use of alternative features may not be enough to attain a viable real-time solution. This may occur if the image feature extraction process must

A.M.G. Tommaselli is with the Departamento de Cartografia, Universidade Estadual Paulista, Rua Roberto Simonsen, 305, 10060-900 Presidente Prudente, São Paulo, Brazil.

C.L. Tozzi is with the Departamento de Engenharia da Computação e Automação Industrial, Faculdade de Engenharia Elétrica, Universidade Estadual de Campinas, Cidade Universitária Zeferino Vaz, C.P. 6101, 13081-970 Campinas, São Paulo, Brazil.

Photogrammetric Engineering & Remote Sensing, Vol. 62, No. 1, January 1996, pp. 57–66.

0099-1112/96/6201-57$3.00/0

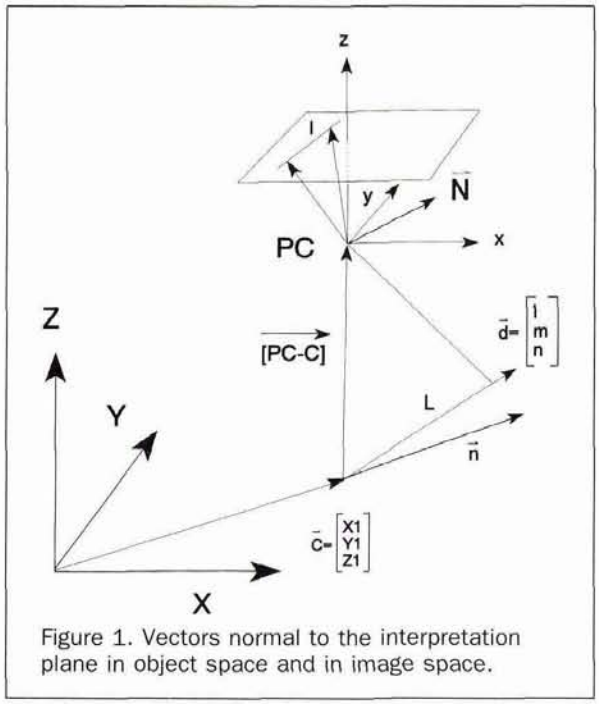

Figure 1. Vectors normal to the interpretation plane in object space and in image space.

be applied over the full image, resulting in a time consuming process.

Some authors have proposed the use of parallel processing techniques or hardware implemented solutions to remove this bottleneck. These solutions, however, are costly, equipment dependent, and cannot be generalized.

The concept of Verification Vision can be used as an additional approach to increase the throughput of the system. According to Feddema *et al.* (1991), "the purpose of Verification Vision is not to recognize objects but to verify and update the location of the objects based on a selected number of image features." If the object model is known and an estimated camera position and orientation are available, the position of the selected feature can be predicted and the feature extraction process is applied only to a small window enclosing the feature, instead of to the whole image.

In "eye-in-hand" robot vision systems, a good estimate for the camera location parameters is always available from the kinematics model of the manipulator (Paul, 1981), and the concepts of Verification Vision can be directly applied.

An additional improvement in the concept of Verification Vision can be obtained using filtering techniques (Tommaselli and Tozzi, 1992). Filtering techniques offer two great advantages when applied to the dynamic space resection problem in eye-in-hand robot vision systems:

- Parameter estimation can be achieved using past observations with no necessity of storing them; and
- If convergence is assured, the camera location parameter estimates are recursively improved for each new observation introduced.

This recursive filtering approach, associated with the concept of Verification Vision, can be used to feedback to the feature extraction step to reduce the search space and, hence, to decrease computational efforts. The better the camera location estimate, the smaller are the window to be processed and the computational effort needed for feature extraction.

Sequential procedures were extensively studied by the photogrammetric community in the problem of on-line triangulation. Gruen (1985) discussed some aspects of sequential algorithms, emphasizing the Kalman Covariance Update, the Triangular Factor Update, and the Givens Transformations Update. The advantages of the Triangular Factor Update were also reported by Gruen (1982).

The main objective of this work is to present a photogrammetric approach to space resection using the concept of Verification Vision, as stated above. A mathematical model for the correspondence of a straight line in the object and image spaces is adopted (Tommaselli and Tozzi, 1992). Kalman Filtering is applied to the camera parameter estimation process, and it is shown that a feedback of the estimated camera parameters into the image feature extraction process leads to a global reduction in the computational effort.

In the next section, the adopted mathematical model is presented. The proposed recursive procedure, the application of Kalman Filtering, and the feature extraction methodology are then described. Finally, results with simulated and real data are discussed and conclusions are presented.

The Mathematical Model for the Space Resection Solution

The mathematical model adopted for the solution of the space resection problem using straight lines is based on the equivalence between the vector normal to the interpretation plane in the image space and the vector normal to the rotated interpretation plane in the object space (Tommaselli and Tozzi, 1992). The interpretation plane is defined as being the plane which contains the straight line in the object space (L), the projected straight line in the image space (l), and the perspective center (PC) of the camera (see Figure 1).

The vector normal to the interpretation plane in the image space is given by

$$\mathbf{N} = -\begin{bmatrix} f.\cos\theta \\ f.\sin\theta \\ -\rho \end{bmatrix} \tag{1}$$

where f is the focal length and θ and ρ are the parameters of the straight line in the image plane, using its normal representation ($\cos\theta.x + \sin\theta.y - \rho = 0$).

The vector $\mathbf{n}$, normal to the interpretation plane in the object space, is defined by the vector product of the direction vector of the straight line ($\mathbf{d}$) and the vector difference ($\mathbf{PC} - \mathbf{C}$) (see Figure 1): i.e.,

$$\mathbf{n} = \begin{bmatrix} n_x \\ n_y \\ n_z \end{bmatrix} = \mathbf{d} \times [\mathbf{PC} - \mathbf{C}]$$

$$= \begin{bmatrix} -n.(Y_c - Y_1) + m.(Z_c - Z_1) \\ n.(X_c - X_1) + l.(Z_c - Z_1) \\ -m.(X_c - X_1) + l.(Y_c - Y_1) \end{bmatrix} \tag{2}$$

where

X_c, Y_c, Z_c are the coordinates of the perspective center of the camera;

X_1, Y_1, Z_1 are the three-dimensional coordinates of a known point on the straight line; and

l, m, n are the components of the direction vector $\mathbf{d}$ of the straight line; all defined in the object space reference system.

Multiplying vector $\mathbf{n}$ by the rotation matrix $\mathbf{R}$ eliminates the angular differences between the object and the image reference systems and results in a vector normal to the interpretation plane in object space that has the same orientation as vector $\mathbf{N}$, normal to the interpretation plane in the image space, but different in magnitude. Thus,

$$\mathbf{N} = \lambda\, \mathbf{R}\, \mathbf{n} \tag{3}$$

where λ is a scale factor, defined by $\lambda = \|\mathbf{N}\|/\|\mathbf{n}\|$, and $\mathbf{R}$ is the rotation matrix,

$$\begin{bmatrix} \cos\phi.\cos\kappa & \cos\omega.\sin\kappa+\sin\omega.\sin\phi.\cos\kappa & \sin\omega.\sin\kappa-\cos\omega.\sin\phi.\cos\kappa \\ -\cos\phi.\sin\kappa & \cos\omega.\cos\kappa-\sin\omega.\sin\phi.\sin\kappa & \sin\omega.\cos\kappa+\cos\omega.\sin\phi.\sin\kappa \\ \sin\phi & -\sin\omega.\cos\phi & \cos\omega.\cos\phi \end{bmatrix} \quad (4)$$

defined by the sequence $M_z(\kappa)\ M_y(\phi)\ M_x(\omega)$ of rotations.

Using Equations 1 and 2, Equation 3 can be rewritten as

$$\begin{bmatrix} f\cdot\cos\theta \\ f\cdot\sin\theta \\ -\rho \end{bmatrix} = -\lambda \begin{bmatrix} r_{11}\cdot n_x + r_{12}\cdot n_y + r_{13}\cdot n_z \\ r_{21}\cdot n_x + r_{22}\cdot n_y + r_{23}\cdot n_z \\ r_{31}\cdot n_x + r_{32}\cdot n_y + r_{33}\cdot n_z \end{bmatrix} \quad (5)$$

where the r_{ij}'s are the elements of the rotation matrix $\mathbf{R}$, as defined in Equation 4.

In the above equations, λ can be eliminated by algebraic manipulation. In order to avoid divisions by zero, Equation 5 is split into two sets of equations, according to the value of parameter θ (orientation of the straight line in the image): i.e.,

for $45° < \theta \le 135°$ or $225° < \theta \le 315°$,

$$\cot\theta = \frac{r_{11}\cdot n_x + r_{12}\cdot n_y + r_{13}\cdot n_z}{r_{21}\cdot n_x + r_{22}\cdot n_y + r_{23}\cdot n_z} \quad (6)$$
$$\frac{-\rho}{f\cdot\sin\theta} = \frac{r_{31}\cdot n_x + r_{32}\cdot n_y + r_{33}\cdot n_z}{r_{21}\cdot n_x + r_{22}\cdot n_y + r_{23}\cdot n_z}$$

Using the relationships between the elements of the normal vector and the parametric representation of the straight line in the image, Equation 6 can be rewritten as

$$a = -\frac{r_{11}\cdot n_x + r_{12}\cdot n_y + r_{13}\cdot n_z}{r_{21}\cdot n_x + r_{22}\cdot n_y + r_{23}\cdot n_z} \quad (7)$$
$$b = -f\cdot\frac{r_{31}\cdot n_x + r_{32}\cdot n_y + r_{33}\cdot n_z}{r_{21}\cdot n_x + r_{22}\cdot n_y + r_{23}\cdot n_z}$$

where the elements of the parametric equation ($y = a.x + b$) are

$$a = -\cot\theta \text{ and } b = \rho/\sin\theta$$

and, for $0° < \theta \le 45°$ or $135° < \theta \le 225°$ or $315° < \theta \le 360°$,

$$\tan\theta = \frac{r_{21}\cdot n_x + r_{22}\cdot n_y + r_{23}\cdot n_z}{r_{11}\cdot n_x + r_{12}\cdot n_y + r_{13}\cdot n_z} \quad (8)$$
$$\frac{-\rho}{f\cdot\cos\theta} = \frac{r_{31}\cdot n_x + r_{32}\cdot n_y + r_{33}\cdot n_z}{r_{11}\cdot n_x + r_{12}\cdot n_y + r_{13}\cdot n_z}$$

In this case, a new parameterization for the straight line must be introduced: i.e.,

$$x = a^*.y + b^* \quad (9)$$

where

$$a^* = -\tan\theta \text{ and} \quad (10)$$

$$b^* = \rho/\cos\theta \quad (11)$$

From Equations 10 and 11, Equation 8 can be rewritten as

$$a^* = -\frac{r_{21}\cdot n_x + r_{22}\cdot n_y + r_{23}\cdot n_z}{r_{11}\cdot n_x + r_{12}\cdot n_y + r_{13}\cdot n_z} \quad (12)$$
$$b^* = -f\frac{r_{31}\cdot n_x + r_{32}\cdot n_y + r_{33}\cdot n_z}{r_{11}\cdot n_x + r_{12}\cdot n_y + r_{13}\cdot n_z}$$

Space Resection Using Straight Lines and Kalman Filtering

In this section, the main steps of the recursive approach for the solution of the space resection problem using straight lines and Kalman Filtering are presented. The aim of this approach is the reduction of the computational cost at the level of image segmentation.

It is assumed that

- The inner orientation parameters of the camera are stable and they are previously determined using a self-calibrating bundle adjustment, with convergent cameras;
- The object model is known, i.e., for each straight line in the object, the coordinates of its two endpoints are known in the object reference system, and these values are supposed to be free of errors; and
- At an initial time, an *a priori* estimate for the location and orientation parameters is available. In the case of space resection, these *a priori* estimates are obtained using the robot kinematics. In the case of object location, some probable position must be computed in the recognition step.

Let $\mathbf{x}_k = [\kappa, \phi, \omega, X_c, Y_c, Z_c]^T$ be the state vector defining the camera position and orientation at time t_k and $\mathbf{P}_k$ its covariance matrix, and let $\mathbf{z}_k^j = [a,b]^T$ be the observation vector for the j^{th} feature in the image.

The sequence of steps for the proposed recursive approach to the solution of the space resection problem is described below (see Figure 2):

(1) At the initial time ($t_k = 1$), the *a priori* estimate for state vector $\hat{\mathbf{x}}_{1|0}$ and its covariance matrix $\mathbf{P}_{1|0}$ are assigned to variables $\hat{\mathbf{x}}_{1|k-1}$ and $\mathbf{P}_{1|k-1}$, respectively;

(2) Using the predicted state vector estimate $\hat{\mathbf{x}}_{1|k-1}$, a perspective transformation is applied to the endpoints of all straight lines in the object model. Hidden lines of the projected object model must be excluded; there are several "hidden lines" algorithms which can be used. It seems that in less complex environments the early Roberts algorithm is appropriate for this task (Rogers, 1985). The visible lines are la-

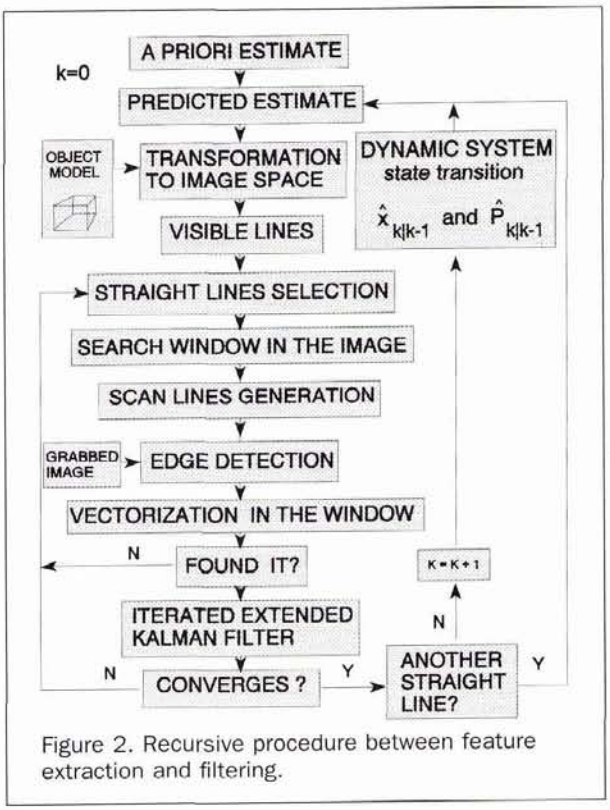

Figure 2. Recursive procedure between feature extraction and filtering.

beled. Predicted values for θ and ρ are computed for the j^{th} line;

(3) A search window is computed using the projected endpoints of the j^{th} straight line. The corners of the search window are defined taking into account the covariance matrix of the predicted state estimate $\mathbf{P}_{1|k-1}$ and the straight line length. This is done using covariance propagation and the collinearity equations;

(4) From the polygon that defines the window, the limits of the scan lines are computed;

(5) Edges are then detected in the search window using the Sobel operators (this step is omitted if an edge image is already available);

(6) The observation vector $\mathbf{z}_k^j$ is obtained from the edge subimage using vectorization techniques, e.g., the Hough transform (Ballard and Brown, 1982) or $\theta - \rho$ grouping (Dudani and Luk, 1978). Systematic errors are eliminated at this step using precomputed calibration parameters. If more than one line is detected within the search window, the predicted values for θ and ρ computed in Step 2 are used for the selection of the most probable one;

(7) The Iterated Extended Kalman Filter is applied and a state estimate $\hat{\mathbf{x}}_{1|k}$ and its covariance matrix $\mathbf{P}_{1|k}$ are computed using the observation vector $\mathbf{z}_k^j$ obtained in the previous step;

(8) The filtered state parameters and their covariance matrix obtained using the j^{th} observation is considered as a predicted value for the $(j+1)^{th}$ observation, and the algorithm proceeds on to Step 2.

The filtered state parameters and their covariance matrix obtained using the j^{th} observation are used as the predicted values for the $(j+1)^{th}$ observation to update the perspective transformation from object to image space. After each iteration, the filtered state parameters obtained are better than the previous ones; hence, the displacement between the acquired image feature and the projected one is progressively reduced, resulting in a reduction of the search window. This procedure is repeated until all available lines have been processed.

If a dynamic process is considered, a prediction $\hat{\mathbf{x}}_{k+1|k}$ and $\mathbf{P}_{k+1|k}$ for the next time t_{k+1} is established using the available estimates and the system model. In the case of robot applications, the joint control parameters can be measured, and the differential changes in the state are predicted using the Jacobian (Paul, 1981). An error estimate for this prediction may be computed if robot joint uncertainties are known.

The IEKF Applied to the Resection Problem

The IEKF (Iterated Extended Kalman Filtering) is a recursive method for state estimation, which enables an observation to be processed once it becomes available. This property makes feasible the proposed recursive strategy in which feature extraction in the image is improved by better state estimates.

In Appendix A, a short review of the IEKF equations is presented. A more detailed description can be found, for example, in Jazwinski (1970).

The application of the IEKF to the space resection model results in the following dimensions for matrices and vectors:

$$ {}_6\mathbf{x}_1 \quad {}_6\eta_1 \quad {}_2\mathbf{M}_2 \quad {}_6\mathbf{P}_6 \quad {}_6\mathbf{K}_2 \quad {}_2\mathbf{z}_1 $$

where

$\hat{\mathbf{x}}_k = [\kappa, \phi, \omega, X_c, Y_c, Z_c]^T$ is the state vector at time t_k,
$\mathbf{z}_k$ are the observations at time t_k,
η is an iterator,
$\mathbf{K}$ is the Kalman gain matrix,
$\mathbf{M}$ is the partial derivatives matrix, and
$\mathbf{P}$ is the state covariance matrix.

The rotation matrix (Equation 4) can be subdivided into three row vectors: i.e.,

$$ \begin{aligned} \mathbf{R}_1 &= [r_{11}\ r_{12}\ r_{13}] \\ \mathbf{R}_2 &= [r_{21}\ r_{22}\ r_{23}] \\ \mathbf{R}_3 &= [r_{31}\ r_{32}\ r_{33}] \end{aligned} \tag{13} $$

Using this notation, Equations 7 and 12 can be rewritten as

$$ \begin{aligned} a &= -\frac{r_{11}\cdot n_x + r_{12}\cdot n_y + r_{13}\cdot n_z}{r_{21}\cdot n_x + r_{22}\cdot n_y + r_{23}\cdot n_z} = -\frac{\mathbf{R}_1\cdot\mathbf{n}}{\mathbf{R}_2\cdot\mathbf{n}} \\ b &= -f\cdot\frac{r_{31}\cdot n_x + r_{32}\cdot n_y + r_{33}\cdot n_z}{r_{21}\cdot n_x + r_{22}\cdot n_y + r_{23}\cdot n_z} = -f\cdot\frac{\mathbf{R}_3\cdot\mathbf{n}}{\mathbf{R}_2\cdot\mathbf{n}} \end{aligned} \tag{14} $$

$$ \begin{aligned} a^* &= -\frac{r_{21}\cdot n_x + r_{22}\cdot n_y + r_{23}\cdot n_z}{r_{11}\cdot n_x + r_{12}\cdot n_y + r_{13}\cdot n_z} = -\frac{\mathbf{R}_2\cdot\mathbf{n}}{\mathbf{R}_1\cdot\mathbf{n}} \\ b^* &= -f\cdot\frac{r_{31}\cdot n_x + r_{32}\cdot n_y + r_{33}\cdot n_z}{r_{11}\cdot n_x + r_{12}\cdot n_y + r_{13}\cdot n_z} = -f\cdot\frac{\mathbf{R}_3\cdot\mathbf{n}}{\mathbf{R}_1\cdot\mathbf{n}} \end{aligned} \tag{15} $$

where f is the camera focal length, $\mathbf{n}$ is the vector normal to the interpretation plane in the object space, and a and b (a^* and b^*) are the observations, defined as

$$ \begin{aligned} a &= G_1(\mathbf{x}_k) = -\frac{\mathbf{R}_1\cdot\mathbf{n}}{\mathbf{R}_2\cdot\mathbf{n}} = -\frac{v}{u} \\ b &= G_2(\mathbf{x}_k) = -f\cdot\frac{\mathbf{R}_3\cdot\mathbf{n}}{\mathbf{R}_2\cdot\mathbf{n}} = -f\cdot\frac{w}{u} \end{aligned} \tag{16} $$

$$ \begin{aligned} a^* &= F_1(\mathbf{x}_k) = -\frac{\mathbf{R}_2\cdot\mathbf{n}}{\mathbf{R}_1\cdot\mathbf{n}} = -\frac{u}{v} \\ b^* &= F_2(\mathbf{x}_k) = -f\cdot\frac{\mathbf{R}_3\cdot\mathbf{n}}{\mathbf{R}_1\cdot\mathbf{n}} = -f\cdot\frac{w}{v} \end{aligned} \tag{17} $$

For the measurement model as stated in Equation 15, the $\mathbf{M}$ matrix (Equation A6, Appendix A), defined by the partial derivatives of the measurement model with respect to the elements of the state vector, is written as

$$ \mathbf{M} = \begin{bmatrix} \frac{\partial F_1}{\partial\kappa} & \frac{\partial F_1}{\partial\phi} & \frac{\partial F_1}{\partial\omega} & \frac{\partial F_1}{\partial X_c} & \frac{\partial F_1}{\partial Y_c} & \frac{\partial F_1}{\partial Z_c} \\ \frac{\partial F_2}{\partial\kappa} & \frac{\partial F_2}{\partial\phi} & \frac{\partial F_2}{\partial\omega} & \frac{\partial F_2}{\partial X_c} & \frac{\partial F_2}{\partial Y_c} & \frac{\partial F_2}{\partial Z_c} \end{bmatrix} $$

where

$$ \frac{\partial F_1}{\partial x_i} = -\frac{\mathbf{R}_2'\cdot\mathbf{n}\cdot\mathbf{R}_1\cdot\mathbf{n} - \mathbf{R}_2\cdot\mathbf{n}\cdot\mathbf{R}_1'\cdot\mathbf{n}}{(\mathbf{R}_1\cdot\mathbf{n})^2}, $$

$$ \frac{\partial F_2}{\partial x_i} = -f\cdot\frac{\mathbf{R}_3'\cdot\mathbf{n}\cdot\mathbf{R}_1\cdot\mathbf{n} - \mathbf{R}_3\cdot\mathbf{n}\cdot\mathbf{R}_1'\cdot\mathbf{n}}{(\mathbf{R}_1\cdot\mathbf{n})^2}, $$

and x_i is an element of the state vector.

The derivatives of the rotation matrix with respect to state elements are

$$ \frac{\partial\mathbf{R}_1}{\partial\kappa} = \mathbf{R}_2, \quad \frac{\partial\mathbf{R}_1}{\partial\phi} = -\mathbf{R}_3\cdot c\kappa, \quad \frac{\partial\mathbf{R}_1}{\partial\omega} = [0\ -r_{13}\ r_{12}], $$

$$ \frac{\partial\mathbf{R}_2}{\partial\kappa} = -\mathbf{R}_1, \quad \frac{\partial\mathbf{R}_2}{\partial\phi} = \mathbf{R}_3\cdot s\kappa, \quad \frac{\partial\mathbf{R}_2}{\partial\omega} = [0\ -r_{23}\ r_{22}], $$

$$ \frac{\partial\mathbf{R}_3}{\partial\kappa} = 0, \quad \frac{\partial\mathbf{R}_3}{\partial\phi} = [c\phi\ \ s\omega\cdot s\phi\ \ -c\omega\cdot s\phi], \quad \frac{\partial\mathbf{R}_3}{\partial\omega} = [0\ -r_{33}\ -r_{32}] $$

where $ci = \cos i$ and $si = \sin i$.

The partial derivatives of the measurement model (Equation 15) with respect to the rotations are

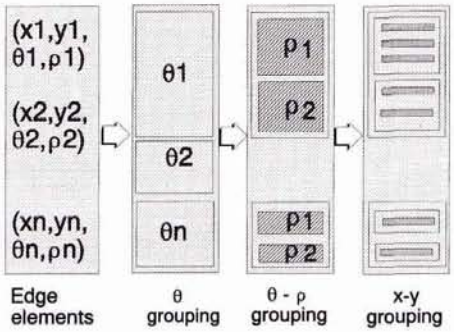

Figure 3. Steps in the θ-ρ grouping (Dudani and Luk, 1978).

$$\frac{\partial F_1}{\partial \kappa} = 1 + \frac{u^2}{v^2}, \qquad \frac{\partial F_2}{\partial \kappa} = f \cdot \frac{w \cdot u}{v^2},$$

$$\frac{\partial F_1}{\partial \phi} = -\frac{(s\kappa \cdot w \cdot v + c\kappa \cdot w \cdot u)}{v^2},$$

$$\frac{\partial F_2}{\partial \phi} = -f \cdot \frac{(c\phi \cdot n_x + s\omega \cdot s\phi \cdot n_y - c\omega \cdot s\phi \cdot n_z) \cdot v + c\kappa^2 \cdot w}{v^2},$$

$$\frac{\partial F_1}{\partial \omega} = -\frac{(-r_{23} \cdot n_y + r_{22} \cdot n_z) \cdot v - u \cdot (-r_{13} \cdot n_y + r_{12} \cdot n_z)}{v^2},$$

$$\frac{\partial F_2}{\partial \omega} = -f \cdot \frac{(-r_{33} \cdot n_y + r_{32} \cdot n_z) \cdot v - w \cdot (-r_{13} \cdot n_y + r_{12} \cdot n_z)}{v^2}.$$

The partial derivatives of the measurement model (Equation 15) with respect to the translations are

$$\frac{\partial F_1}{\partial X_c} = -\frac{\frac{\partial u}{\partial X_c} v - u \frac{\partial v}{\partial X_c}}{v^2}, \quad \frac{\partial F_1}{\partial Y_c} = -\frac{\frac{\partial u}{\partial Y_c} v - u \frac{\partial v}{\partial Y_c}}{v^2},$$

$$\frac{\partial F_1}{\partial Z_c} = -\frac{\frac{\partial u}{\partial Z_c} v - u \frac{\partial v}{\partial Z_c}}{v^2}, \quad \frac{\partial F_2}{\partial X_c} = -f \cdot \frac{\frac{\partial w}{\partial X_c} v - w \frac{\partial v}{\partial X_c}}{v^2},$$

$$\frac{\partial F_2}{\partial Y_c} = -f \cdot \frac{\frac{\partial w}{\partial Y_c} v - w \frac{\partial v}{\partial Y_c}}{v^2}, \quad \frac{\partial F_1}{\partial Z_c} = -f \cdot \frac{\frac{\partial w}{\partial Z_c} v - w \frac{\partial v}{\partial Z_c}}{v^2}$$

where

$$\frac{\partial u}{\partial X_c} = (-r_{22} \cdot n + r_{23} \cdot m), \frac{\partial u}{\partial Y_c} = (r_{21} \cdot n - r_{23} \cdot l), \frac{\partial u}{\partial Z_c} = (-r_{21} \cdot m + r_{22} \cdot l),$$

$$\frac{\partial v}{\partial X_c} = (-r_{12} \cdot n + r_{13} \cdot m), \frac{\partial v}{\partial Y_c} = (r_{11} \cdot n - r_{13} \cdot l), \frac{\partial v}{\partial Z_c} = (-r_{11} \cdot m + r_{12} \cdot l),$$

$$\frac{\partial w}{\partial X_c} = (-r_{32} \cdot n + r_{33} \cdot m), \frac{\partial w}{\partial Y_c} = (r_{31} \cdot n - r_{33} \cdot l), \frac{\partial w}{\partial Z_c} = (-r_{31} \cdot m + r_{32} \cdot l).$$

The partial derivatives for the measurement model as defined by Equation 14 are obtained similarly.

Feature Extraction

The feature extraction step is a key procedure in the proposed recursive approach. Once a state estimate is available (either an "*a priori*" estimate or a filtered estimate), the definition of a search window in the image space is feasible. The main goal of the feature extraction process is to find a straight line in the image which corresponds to a straight line in object space.

For the edge detection, it is assumed that spatial discontinuities result in gray-level discontinuities in the image. The edges in the image are detected using the Sobel operators. Furthermore, the gradient direction is computed from these operators, but using a 5 by 5 window, in order to increase the precision (Kittler *et al.*, 1987).

The edges can be detected in the whole image or for the defined search window. The elements which have a gradient magnitude greater than a defined threshold are considered as belonging to an edge. In order to connect these elements, a vectorization procedure is used.

The θ-ρ grouping method (Dudani and Luk, 1978) was adapted for our approach because only one straight line is selected at a time. In this method, edge pixels are classified using three grouping steps, known as θ-, ρ-, and xy-grouping. The θ-grouping gathers the edge pixels that have gradient directions within a specific angular range, e.g., θ_1 to θ_2, selected based on the θ distribution; the ρ-grouping classify the edge pixels of θ groups according to their ρ-values (computed for each pixel using the equation $\rho = x.\cos\theta + y.\sin\theta$); and the xy-grouping verify discontinuities within each θ-ρ group (Figure 3).

There could be several lines within a window but only one corresponding to the selected object straight line. The proposed adaptation is summarized in Figure 4. A histogram of the θ values is generated, scanning for the edge pixels over the search window. The peaks in this histogram are compared with the predicted θ value and the nearest value is chosen. A θ group is defined by the edge pixels which have θ values within an interval, centered in the chosen peak of the histogram, and bounded by pre-defined limits, consistent with the precision of the gradient detection method. Then, the search window is scanned and a ρ histogram is generated, using only the edge pixels in the selected θ group. The peaks in the ρ histogram are analyzed to find the closest to the predicted ρ. Finally, the edge pixels which are within the θ-ρ intervals are grouped. The edge image is directly used in the adapted θ-ρ procedure with no further processing. For a selected θ-ρ group, only the pixel with the highest gradient magnitude is selected in each scan line.

The edge pixel coordinates are defined in the frame buffer reference system. These coordinates must be transformed (scaled and translated) to an approximated center of the image. The systematic errors are corrected using Equations 18: i.e.,

$$x_i = x_f - c_x + (x_f - c_x)(k_1 \cdot r^2) + (x_f - c_x) \cdot d_x \qquad (18)$$
$$y_i = y_f - c_y + (y_f - c_y)(k_1 \cdot r^2)$$

where

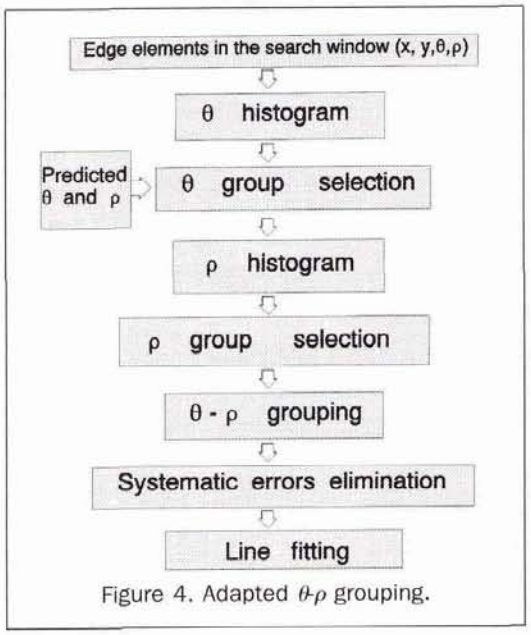

Figure 4. Adapted θ-ρ grouping.

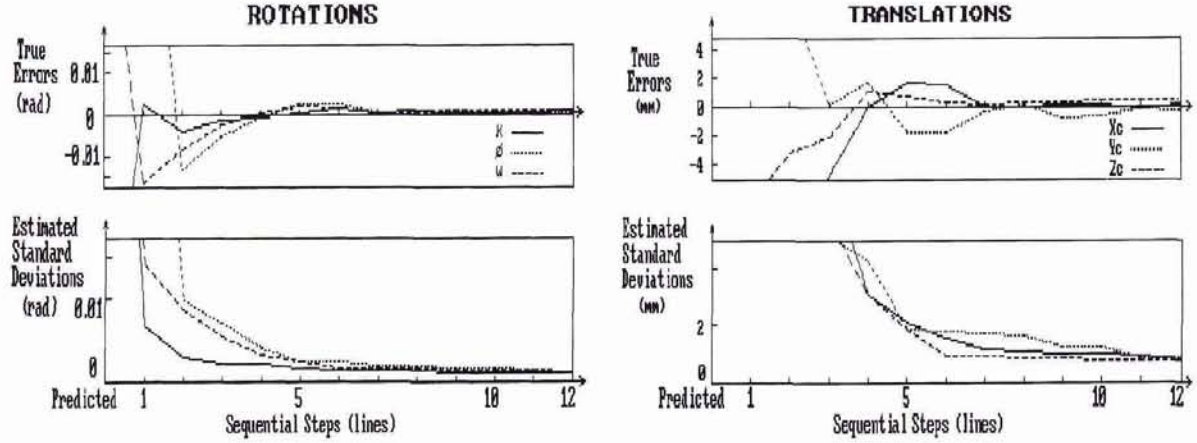

Figure 5. Error analysis for a space resection using straight lines.

x_i and y_i are the image coordinates of a pixel related to the principal point (image center); and

c_x, c_y, k_1, and d_s are the inner orientation parameters, obtained from a previous camera calibration, where c_x and c_y are the image coordinates of the principal point; k_1 is the coefficient of radial distortion (higher order coefficients and decentering distortion are neglected); and d_s is the scale factor in x.

A least-squares adjustment is used to fit a straight line to the selected set of image edge points with subpixel precision. As observed earlier for the mathematical model, two sets of equations must be defined and used according to the θ value. These equations are derived from the least-squares solution, considering the pixel x (or y) coordinate free of errors.

For $45° < \theta \leq 135°$ or $225° < \theta \leq 315°$,

$$a = \frac{1}{\det} \cdot (N \cdot \sum x_i \cdot y_i - \sum x_i \cdot \sum y_i)$$
$$b = \frac{1}{\det} \cdot (- \sum x_i \cdot \sum x_i \cdot y_i + \sum x_i^2 \cdot \sum y_i) \quad (19)$$

where N is the number of pixels and $\det = (N \cdot \sum x_i^2 - \sum x_i \cdot \sum x_i)$. The a and b variances are given by

$$\sigma_a^2 = \frac{N}{\det} \quad \text{and} \quad \sigma_b^2 = \frac{\sum x_i^2}{\det} \quad (20)$$

For $0° < \theta \leq 45°$ or $135° < \theta \leq 225°$ or $315° < \theta \leq 360°$,

$$a^* = \frac{1}{\det^*} \cdot (N \cdot \sum x_i \cdot y_i - \sum y_i \cdot \sum x_i)$$
$$b^* = \frac{1}{\det^*} \cdot (- \sum y_i \cdot \sum x_i \cdot y_i + \sum y_i^2 \cdot \sum x_i) \quad (21)$$

where $\det^* = (N \cdot \sum y_i^2 - \sum y_i \cdot \sum y_i)$. Similarly, a^* and b^* variances are given by

$$\sigma_{a^*}^2 = \frac{N}{\det} \quad \text{and} \quad \sigma_{b^*}^2 = \frac{\sum y_i^2}{\det} \quad (22)$$

In order to avoid gross errors, the residuals are computed and verified after line fitting, eliminating the pixel with the largest residual, and then performing a new line fitting. This process is repeated until a predefined number of points remains in the set and the residuals are larger than a defined threshold. If large residuals still remain for the defined minimum number of points, a straight line error vectorization is assumed.

The variances obtained from Equations 20 and 22 are measurements of precision, indicating only the scattering in the line fitting. However, in addition to the scattering in the line fitting, errors in the inner orientation parameters (mainly in the principal point) must be taken into account in the computation of covariance matrix **R**. This can be done by covariance propagation techniques, as discussed next.

Suppose that the a and b parameters are computed as a function of two point's coordinates (x_1, y_1) and (x_2, y_2). Then

$$a = \frac{(y_2 - y_1)}{(x_2 - x_1)} \qquad b = \frac{(y_1 \cdot x_2 - x_1 \cdot y_2)}{(x_2 - x_1)} \quad (23)$$

If coordinates (x_1, y_1) and (x_2, y_2) are affected by systematic errors, then Equation 23 can be rewritten as Equations 24 and 25: i.e.,

$$a' = \frac{(y_2 - c_y - (y_1 - c_y))}{(x_2 - c_x + (x_2 - c_x)\, d_s - x_1 + c_x - (x_1 - c_x)\, d_s)} = \frac{a}{(1 + d_s)} \quad (24)$$

$$b' = b + a \cdot c_x - c_y \quad (25)$$

With these corrections, parameters a' and b' are obtained. The effect of an error in the radial lens distortion (k_1) was neglected due to the small magnitude of this error.

Similarly, for $0° < \theta \leq 45°$ or $135° < \theta \leq 225°$ or $315° < \theta \leq 360°$,

$$a^* = \frac{(x_2 - x_1)}{(y_2 - y_1)} \qquad b^* = \frac{(x_1 \cdot y_2 - y_1 \cdot x_2)}{(y_2 - y_1)} \quad (26)$$

$$a^{*'} = a^* \cdot (1 + d_s) \quad (27)$$

$$b^{*'} = (b^* - c_x + a^* \cdot c_y)\,(1 + d_s) \quad (28)$$

As the parameters a and b (or a^* and b^*) are computed using line fitting, the following equations, derived by the covariance propagation method, must be used to determine the variances of the a' and b' parameters:

$$\sigma_{a'}^2 = \frac{1}{(1 + d_s)^2}\,\sigma_a^2 + \frac{a^2}{(1 + d_s)^4}\,\sigma_{d_s}^2 \quad (29)$$

$$\sigma_{b'}^2 = c_x^2 \cdot \sigma_a^2 + \sigma_b^2 + a^2 \cdot \sigma_{c_x}^2 + \sigma_{c_y}^2 \quad (30)$$

and, for $a^{*'}$ and $b^{*'}$,

$$\sigma^2_{a^{*'}} = (1 + d_s)^2 \cdot \sigma^2_{a^*} + a^{*2} \cdot \sigma^2_{d_s} \quad (31)$$

$$\sigma^2_{b^{*'}} = (1 + d_s)^2 (c_y^2 \sigma^2_{a^*} + \sigma^2_{b^*} + \sigma^2_{c_x} + a^{*2} \sigma^2_{c_y}) + (b^* - c_x + a^* c_y) \sigma^2_{d_s} \quad (32)$$

Equations 29 to 32 enable the computation of the accuracy of the straight line fitting in the image, considering both the scattering of the edge pixels and the effects of the errors in the inner orientation parameters (except k_1).

Results

In this section, results obtained with the proposed recursive procedure using simulated and real data are presented and discussed.

Procedures for Simulated Data Generation

The inner orientation parameters of the camera were assumed known. It also was assumed that neither the robot nor the object move during image acquisition. The following parameters for the simulated camera were used: 15-mm focal length, 5- by 4-mm^2 imaging area, and 10- by 10-µm^2 pixel size.

For the established exterior camera parameters (position and orientation), the image coordinates corresponding to object points (corners) were computed using the collinearity equations. Random errors with a standard deviation of 3 µm were introduced in the image. This error of 3 µm is equivalent to one-third of the pixel size; this precision for the image coordinates was assumed because straight lines can be extracted with subpixel precision (Liu and Huang, 1991).

The straight line parameters (a-b or a^*-b^*) were finally computed from pairs of points corresponding to the object edges using Equations 23 and 26.

The variances of the straight line parameters in the image (a-b or a^*-b^*) were obtained using covariance propagation. Supposing that $\sigma_x^2 = \sigma_y^2$ and neglecting correlations, the variances of the a and b parameters can be written as

$$\sigma_a^2 = \frac{2(a^2 + 1)}{(x_2 - x_1)^2} \sigma_x^2 \qquad \sigma_b^2 = \frac{(x_2^2 - x_1^2)}{(x_2 - x_1)^2} (a^2 + 1) \sigma_x^2 \quad (33)$$

Similar considerations are used for the a^*-b^* representation: i.e.,

$$\sigma^2_{a^*} = \frac{2(a^{*2} + 1)}{(y_2 - y_1)^2} \sigma_x^2 \qquad \sigma^2_{b^*} = \frac{(y_2^2 - y_1^2)}{(y_2 - y_1)^2} (a^{*2} + 1) \sigma_x^2 \quad (34)$$

Results Obtained from Simulated Data

Extensive simulations were carried out in order to verify the behavior of the proposed model, and the results for a typical situation are described here.

The object reference system was supposed to be coincident with the global reference system. A wireframe cube of 70-mm edge size, 1108 mm away from the origin of the camera reference system, was considered, and simulated data for this configuration was generated as described above. The 12 lines corresponding to the edges of the cube were used (no hidden lines), and estimates for the camera state vector were obtained sequentially.

Figures 5a and 5b show the true errors and estimated standard deviations for the rotation and translation parameters, respectively, for each line processed. The true error (ε_v) is defined as the difference between the estimated and the true parameter values, and the standard deviation (σ_v) is defined as the square root of the estimated variance.

For this configuration, 50 experiments were conducted and the mean-square values for the true error (ε_{vm}) and estimated standard deviation (σ_{vm}) were computed using the last iteration values for each experiment. The results obtained are presented in Table 1.

The following conclusions can be derived from the analysis of the graphics of Figure 5 and the data in Table 1:

- The filter has a strong convergence over the 12 lines. In fact, for the example considered, when the ninth feature was introduced, the filter had already converged to the final values;
- Only four lines are sufficient to obtain a good estimate;
- Parameters k and X_c converge before the others;
- A high accuracy estimation is reached with this approach; for the example considered, rotational and translational standard deviations were smaller than 6 minutes and 1.6 mm, respectively; and
- The estimated standard deviations are consistent with the computed mean-square errors.

Simulations were also carried out for particular situations, such as concentration of observed lines in the corners of the image, deficient configurations of straight lines, outliers in the observations due to wrong correspondence, errors in the inner orientation parameters, and different focal lengths.

Adequate responses were obtained for these situations, showing that the proposed solution can be applied for most of them. These results are omitted due to lack of space.

Results Obtained with Real Data

Experiments with real data using a partially controlled environment were performed in order to verify the accuracy potential of the proposed method.

Images were collected using a Kentec-CCD camera, with 15-mm nominal focal length and grabbed by an AT-Vista board, installed in an AT-386 computer. Although the images were grabbed with 512 by 400 by 8 bits, only the 200 even lines were used in order to speed up the whole process.

The inner orientation parameters were obtained using a self-calibrating bundle adjustment, with the six convergent images taken from a set of 20 circular targets and with the principal point related to the approximated center of the frame buffer (256, 200). The values of the calibrated inner orientation parameters and their standard deviations are presented in Table 2.

The edge images were obtained off-line using the Sobel operators and computing the gradient direction with a 5 by 5 window; the edge image was stored in the memory when the recursive procedure was performed. Values for the scattering in the line fitting procedure were considered in the range 10 µm to 1 µm, depending on the quality of the image. The variance considered for the observations also takes into account the errors in the inner orientation parameters.

In a typical experiment the camera was installed on a tripod, observing a cube of 70 mm. During image acquisition, the camera and the object were motionless. *A priori* estimates for the external orientation parameters were approximately measured in the experimental set (predicted values). The original picture and the edge image for a cube 1.12 m

TABLE 1. RESULTS OBTAINED FROM THE SIMULATION OF THE WIREFRAME CUBE

	True Value	Predicted Estimate	Predicted Variance	ε_{vm}	σ_{vm}
κ	2.8 rad	2.72	$(0.086)^2$	−0.00195	0.00152
ϕ	0.5 rad	0.56	$(0.086)^2$	−0.00130	0.00154
ω	−1.17 rad	−1.10	$(0.086)^2$	0.00185	0.00161
X_c	540. mm	548.	$(10.0)^2$	1.460	1.533
Y_c	880. mm	872.	$(10.0)^2$	1.087	1.505
Z_c	400. mm	410.	$(10.0)^2$	1.675	1.486

TABLE 2. INNER ORIENTATION PARAMETERS OF THE CCD CAMERA.

Parameter	c_x (mm)	c_y (mm)	Radial Distortion	x Scale Factor	Focal Length (mm)
Value	−0.1478	0.0487	0.000323	0.06847	16.3896
σ_x	0.0165	0.0191	0.000031	0.00021	0.0633

away from the camera are presented in Figures 6a and 6b, respectively. The results obtained are presented in Table 3.

Reduction of the Feature Searching Space

For the configuration described above, the computing time for each step in the procedure has been determined. Table 4 presents these results for the nine visible edges of the cube. The edges were sorted on the table from left to right according to the sequence in which they were detected in the iterative processing. An AT-386 computer was used for all the calculations. It is worth noting the reduction in the vectorization time once each new observation was processed, whereas the computation time of the other steps, mainly the estimation step, did not change significantly. A picture showing the progressive reduction of the feature searching window for this configuration is presented in Figure 7.

Conclusions

A recursive approach based on straight line correspondences and on state estimation using Kalman Filtering has been presented for the solution of the space resection problem.

The proposed approach was tested using synthetic and real data, and the results obtained confirm its effectiveness.

The most important contributions of the proposed approach are the adoption of an explicit mathematical model using straight lines for the space resection solution; the use of iterative filtering, allowing the progressive improvement of the exterior camera parameter estimation; and progressive reduction of the feature searching space in the image, thus reducing the computational effort at the image processing level and making feasible many applications in the area of robot vision. The obtained accuracy and the processing time show the applicability of the proposed approach in several different tasks related to machine vision and photogrammetry. Further improvements can be obtained using more accurate inner orientation parameters and using more stable and higher resolution CCD cameras. More effective edge detection and vectorization techniques must be studied and applied to this approach.

In the reported experiments, both the camera and the object were static. Other methods of sequential estimation could be applied with some advantages over Kalman Filtering and with the same concept of gradual reduction in image space for feature extraction. However, the original recursive method was proposed to be applied with dynamic problems such as moving objects or robot wrist location; in these cases, Kalman Filtering seems to be suitable.

The presented mathematical model can also be employed in 3D feature reconstruction by computing the intersection of the interpretation planes generated from two (or more) distinct views.

Appendix A

Iterated Extended Kalman Filter (IEKF)

Let Equation A1 be the description of a discrete dynamic stochastic system: i.e.,

$$\mathbf{x}_{k+1} = \phi\,(\mathbf{x}_k,\, t_{k+1},\, t_k) + \Gamma\,(\mathbf{x}_k,\, t_k)\,\mathbf{w}_{k+1} \qquad \text{(A1)}$$

For a linear system,

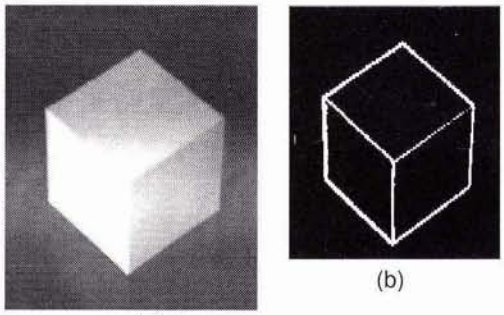

(a) (b)

Figure 6. (a) Picture of a cube 1.12 m away from the camera. (b) Edges of the cube using Sobel operators.

$$\phi\,(\mathbf{x}_k,\, t_{k+1},\, t_k) = \mathbf{F}(t_{k+1},\, t_k)\mathbf{x}_k \qquad \text{(A2)}$$

where

- $\mathbf{x}_k$ is the n-vector state at t_k;
- ϕ is an n-vector state transition function;
- Γ is an (n by r) matrix;
- $\mathbf{w}_k$ is an r-vector, called state transition noise ($\mathbf{w}_k \sim N(0,Q_k)$); and
- $\mathbf{F}$ is an (n by r) matrix of state transition.

Let $\mathbf{z}_k$ be the observation vector: i.e.,

$$\mathbf{z}_k = h(\mathbf{x}_k,\, t_k) + \mathbf{n}_k \qquad k = 1,\, 2,\, \ldots \qquad \text{(A3)}$$

where

- $\mathbf{z}_k$ are the observations at t_k; and
- $\mathbf{n}_k$ is the vector of measurement noise, $\mathbf{n}_k \sim N(0,R_k)$.

Equation (A3) describes the measurement model.

The Kalman filter as originally proposed deals with linear models only. In order to use its approach to a non-linear discrete model, the equations must be extended by Taylor linearization. In the next steps, the equations for the IEKF (Iterated Extended Kalman Filtering) are presented without further development.

The IEKF is based on an iterator which is analyzed for each iteration to verify the filter convergence. This iterator is given by

$$\hat{\eta}_{i+1} = \hat{\mathbf{x}}_{k|k-1} + \mathbf{K}_{k;\eta_i}(\mathbf{z}_k - h(\eta_i,\, t_k) - \mathbf{M}_{k;\eta_i}\,(\hat{\mathbf{x}}_{k|k-1} - \hat{\eta}_i)) \qquad \text{(A4)}$$

where $(\mathbf{z}_k - h(\eta_i,\, t_k) - \mathbf{M}_{k;\eta_i}\,(\hat{\mathbf{x}}_{k|k-1} - \hat{\eta}_i))$ are the predicted residuals; and $\mathbf{K}_{k;\eta_i}$ is the Kalman gain matrix at t_k using estimates for the state vector given by η_i. Kalman gain is expressed by

TABLE 3. PREDICTED AND FINAL FILTERED VALUES OBTAINED USING THE IEKF, FOR A CUBE 1.12 M AWAY FROM THE CAMERA.

	Predicted Values		Filtered Values	
	Predicted State	Standard Deviation	Filtered State	Standard Deviation
κ	2.6070	0.0523	2.577852	0.0015
ϕ rad	0.4870	0.0523	0.469064	0.0013
ω	−0.6280	0.0523	−0.644857	0.0020
X_c	528.00	10.00	523.18	1.45
Y_c mm	628.00	10.00	621.10	1.68
Z_c	785.00	10.00	789.19	1.72

TABLE 4. COMPUTATION TIME, IN SECONDS, FOR EACH STEP OF THE RECURSIVE PROCEDURE, AND SEARCH WINDOW AREA, GIVEN IN PIXELS, FOR EACH STRAIGHT LINE.

Step \ Line	67	74	45	56	52	23	36	41	12
Hidden Lines	0.05	0.06	0.06	0.06	0.06	0.05	0.05	0.06	0.05
Scan Lines	0.11	0.11	0.05	0.05	0.05	0.05	0.05	0.05	0.05
Vectorization	6.31	3.46	1.37	1.43	0.88	0.60	0.55	0.77	0.83
Filtering	0.22	0.22	0.22	0.22	0.28	0.16	0.22	0.17	0.22
Total Time	6.69	3.85	1.70	1.76	1.27	0.86	0.87	1.05	1.15
Window Area	28520	1876	3545	2946	1326	1002	713	581	552

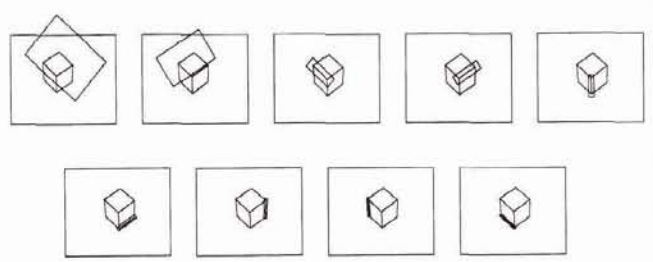

Figure 7. Search window reduction by feedback of the estimation step.

$$\mathbf{K}_{k;\eta_i} = \mathbf{P}_{k|k-1}\mathbf{M}^{\mathrm{T}}_{k;\eta_i}\,(\mathbf{M}_{k;\eta_i}\mathbf{P}^{\mathrm{T}}_{k|k-1}\mathbf{M}_{k;\eta_i}+\mathbf{R}_k^{-1}) \qquad \text{(A5)}$$

where $(\mathbf{M}_{k;\eta_i}\mathbf{P}^{\mathrm{T}}_{k|k-1}\mathbf{M}_{k;\eta_i} + \mathbf{R}_k^{-1})$ is the predicted covariance matrix, and in which

$\mathbf{M}_{k;\eta_i}$ is the partial derivatives matrix of function h with respect to the elements of the state vector

$$\mathbf{M}_{k;\bar{\mathbf{x}}_k} = \left[\frac{\partial h^k\,(\bar{\mathbf{x}}_k,t_k)}{\partial \mathbf{x}_m}\right]; \qquad \text{(A6)}$$

$\mathbf{P}_{k|k-1}$ is the predicted covariance matrix, which is obtained based on the updating of the covariance matrix computed at t_{k-1};

$\hat{\mathbf{x}}_{k|k-1}$ is the predicted state at t_k, based on measurements at t_{k-1} computed using the linearized state transition function; and

η_i is the iterator, which is an estimate for $\hat{\mathbf{x}}_{k|k}$ at t_k.

At the first iteration $\eta_1 = \hat{\mathbf{x}}_{k|k-1}$, which is the predicted state estimate at t_k based on measurements taken at t_{k-1}. The result of the first iteration, η_2, is used in the second iteration and this process is carried out until there is no further improvement in η_i. Thus, the final estimate for $\hat{\mathbf{x}}_{k|k}$ is given by the last iterator η_i.

Because the state estimate has converged, the filtered covariance matrix can be computed and is given by

$$\mathbf{P}_{k|k} = (\mathbf{I}-\mathbf{K}_k\mathbf{M}_k)\mathbf{P}_{k|k-1}\,(\mathbf{I}-\mathbf{K}_k\mathbf{M}_k)^{\mathrm{T}} + \mathbf{K}_k\mathbf{R}_k\mathbf{K}_k^{\mathrm{T}} \qquad \text{(A7)}$$

When multiple uncorrelated observations are available at time t_k, it is possible to compute recursively the estimates for the state at time t_k. This is accomplished by introducing one observation at a time and assuming that $\mathbf{F} = \mathbf{I}$ and $\Gamma = \mathbf{Q} = 0$; that is, the state remains unchanged at t_k and its estimate and covariance matrix are recursively improved for each new observation introduced.

References

Ballard, D.H., and C.M. Brown, 1982. *Computer Vision*, Prentice-Hall, New Jersey, 522 p.

Chen, S.Y., and W.H. Tsai, 1991. Determination of Robot Locations by Common Object Shapes, *IEEE Transactions on Robotics and Automation*, 7(1):149–156.

Chen, W., and B.C. Jiang, 1991. 3-D Camera Calibration Using Vanishing Point Concept, *Pattern Recognition*, 24(1):57–67.

Chen, Z., D. Tseng, and J. Lin, 1989. A Simple Vision Algorithm for 3-D Position Determination using a Single Calibration Object, *Pattern Recognition*, 22(2):173–187.

Dhome, M., M. Richetin, J. Lapresté, and G. Rives, 1989. Determination of the Attitude of 3-D Objects from a Single Perspective View, *IEEE Transactions on PAMI*, 11(12):1265–1278.

Dudani, S.A., and A.L. Luk, 1978. Locating Straight-Line Edge Segments on Outdoor Scenes, *Pattern Recognition*, 10:145–157.

Echigo, T., 1990. A Camera Calibration Technique Using Three Sets of Parallel Lines, *Machine Vision and Applications*, 3:159–167.

Feddema, J.T., C.S.G. Lee, and O.R. Mitchell, 1991. Weighted Selection of Image Features for Resolved Rate Visual Feedback Control, *IEEE Transactions on Robotics and Automation*, 7(1):31–47.

Fischler, A.M., and R.C. Bolles, 1981. Random Sample Consensus: A Paradigm for Model Fitting with Applications to Image Analysis and Automated Cartography, *Communications of the ACM*, 24(6):381–395.

Gruen, A.W., 1982. An Optimum Algorithm for On-Line Triangulation, *Proceedings of the International Society for Photogrammetry and Remote Sensing*, Helsinki, Commission III.

———, 1985. Algorithmic Aspects in On-Line Triangulation, *Photogrammetric Engineering & Remote Sensing*, 51(4):419–436.

———, 1992. Recent Advances of Photogrammetry in Robot Vision, *ISPRS Journal of Photogrammetry and Remote Sensing*, 47:307–323.

Jazwinski, A.H., 1970. *Stochastic Processes and Filtering Theory*, Academic Press, New York, 376 p.

Kittler, J., T. Eggleton, J. Illingworth, and K. Paler, 1987. An Averaging Edge Detector, *Pattern Recognition Letters*, 6(1):27–32.

Lee, R., P.C. Lu, and W.H. Tsai, 1990. Robot Location Using Single Views of Rectangular Shapes, *Photogrammetric Engineering & Remote Sensing*, 56(2):231–238.

Lenz, R.K., and R.Y. Tsai, 1988. Techniques for Calibration of the Scale Factor and Image Center for High Accuracy 3-D Machine Vision Metrology, *IEEE Transactions on PAMI*, 10(5):713–720.

Liu, Y., and T.S. Huang, 1991. Determining Straight Line Correspondences from Intensity Images, *Pattern Recognition*, 24(6):489–504.

Liu Y., T.S. Huang, and O.D. Faugeras, 1990. Determination of Camera Location from 2-D to 3-D Line and Point Correspondences, *IEEE Transactions on PAMI*, 12(1):28–37.

Lugnani, J.B., 1980. *Using Digital Entities as Control*, PhD Thesis, Department of Surveying Engineering, The University of New Brunswick, Fredericton, 159 p.

Mulawa, D.C., and E.M. Mikhail, 1988. Photogrammetric Treatment of Linear Features, *Proceedings of the International Society for Photogrammetry and Remote Sensing*, Kyoto, Commission III, pp. 383–393.

Paul, R.P., 1981. *Robot Manipulators: Mathematics, Programming and Control*, MIT Press, Cambridge, Massachusetts.

Rogers, D.F., 1985. *Procedural Elements for Computer Graphics*, McGraw-Hill, Singapore.

Salari, E., and C. Jong, 1990. A Method to Calculate the Structure and Motion Parameters from Line Correspondences, *Pattern Recognition*, 23(6):553–561.

Tommaselli, A.M.G., and J.B. Lugnani, 1988. An Alternative Mathematical Model to the Collinearity Equation Using Straight Features, *Proceedings of the International Society for Photogrammetry and Remote Sensing*, Kyoto, Commission III, pp. 765–774.

Tommaselli, A.M.G., and C.L. Tozzi, 1992. A Filtering Based Approach to Eye-in-Hand Robot Vision, *Proceedings of the International Society for Photogrammetry and Remote Sensing*, Washington, Commission V, pp. 182–189.

Wang, L.L., and W.H. Tsai, 1990. Computing Camera Parameters Using Vanishing-Line Information from a Rectangular Parallelepiped, *Machine Vision and Applications*, 3:129–141.

(Received 26 October 1993; accepted 13 January 1994; revised 20 June 1994)

Forthcoming Articles

M. Les Bober, Duncan Wood, and *Raymond A. McBride,* Use of Digital Image Analysis and GIS to Assess Regional Soil Compaction Risk.

Michel Boulianne, Rock Santerre, Paul-André Gagnon, and *Clément Nolette,* Floating Lines and Cones for Use as a GPS Mission Planning Aid.

Timothy L. Bowers and *Lawrence C. Rowan,* Remote Mineralogic and Lithologic Mapping of the Ice River Alkaline Complex, British Columbia, Canada, Using AVIRIS Data.

Gregory J. Carbone, Sunil Narumalani, and *Michelle King,* Application of Remote Sensing and GIS Technologies with Physiological Crop Models.

Christopher Deckert and *Paul V. Bolstad,* Forest Canopy, Terrain, and Distance Effects on Global Positioning System Point Accuracy.

Sam Ekstrand, Landsat TM-Based Forest Damage Assessment: Correction for Topographic Effects.

Giles M. Foody, Relating the Land-Cover Composition of Mixed Pixels to Artificial Neural Network Classification Output.

Mark Gahegan and *Julien Flack,* A Model to Support the Integration of Image Understanding Techniques within a GIS.

P. Gong, Integrated Analysis of Spatial Data from Multiple Sources: Using Evidential Reasoning and Artificial Neural Network Techniques for Geological Mapping.

Maurice S. Gyer, Methods for Computing Photogrammetric Refraction Corrections for Vertical and Oblique Photographs.

Christian Heipke, Wolfgang Kornus, and *Anton Pfannenstein,* The Evaluation of MEOSS Airborne Three-Line Scanner Imagery: Processing Chain and Results.

Matthew Heric, Carroll Lucas, and *Christopher Devine,* The Open Skies Treaty: Qualitative Utility Evaluations of Aircraft Reconnaissance and Commercial Satellite Imagery.

Joachim Höhle, Experience with the Production of Digital Orthophotos.

Pamela E. Jansma and *Harold R. Lang,* Applications of Spectral Stratigraphy to Upper Cretaceous and Tertiary Rocks in Southern Mexico: Tertiary Graben Control on Volcanism.

Peter E. Joria and *Janet C. Jorgenson,* Comparison of Three Methods for Mapping Tundra with Landsat Digital Data.

N.G. Kardoulas, A.C. Bird, and *A.I. Lawan,* Geometric Correction of SPOT and Landsat Imagery: A Comparison of Map and GPS Derived Control Points.

Arnon Karnieli, Amnon Meisels, Leonid Fisher, and *Yaacov Arkin,* Automatic Extraction and Evaluation of Geological Linear Features from Digital Remote Sensing Data Using a Hough Transform.

Steven T. Knick, John T. Rotenberry, and *Thomas J. Zarriello,* Supervised Classification of Landsat Thematic Mapper Imagery in a Semi-Arid Rangeland by Nonparametric Discriminant Analysis.

Liang-Hwei Lee and *Tsu-Tse Su,* Vision-Based Image Processing of Digitized Cadastral Maps.

Donald L. Light, Film Cameras or Digital Sensors? The Challenge Ahead for Aerial Imaging.

Paul Pope, Ed Van Eeckhout, and *Cheryl Rofer,* Waste Site Characterization through Digital Analysis of Historical Aerial Photographs.

Donald C. Rundquist, Luoheng Han, John F. Schalles, and *Jeffrey S. Peake,* Remote Measurement of Algal Chlorophyll in Surface Waters: The Case for the First Derivative of Reflectance near 690 NM.

Soren Ryherd and *Curtis Woodcock,* Combining Spectral and Texture Data in the Segmentation of Remotely Sensed Images.

Eric M. Sanden, Carlton M. Britton, and *James H. Everitt,* Total Ground-Cover Estimates from Corrected Scene Brightness Measurements.

Tian-Yuan Shih, The Sign Permutation in the Rotation Matrix and the Formulation of Collinearity and Coplanarity Equations.

Andrew K. Skidmore, Fional Watford, Paisan Luckananurug, and *P.J. Ryan,* An Operational GIS Expert System for Mapping Forest Soils.

Lawrence V. Stanislawski, Bon A. Dewitt, and *Ramesh L. Shrestha,* Estimating Positional Accuracy of Data Layers within a GIS through Error Propagation.

Steve Stehman, Estimating the Kappa Coefficient and Its Variance Under Stratified Random Sampling.

Paul C. Van Deusen, Unbiased Estimates of Class Proportions from Thematic Maps.

A.P. van Deventer, A.D. Ward, P.H. Gowda, and *J.G. Lyon,* Using Thematic Mapper Data to Identify Contrasting Soil Plains and Tillage Practices.

Chris Varekamp, Andrew K. Skidmore, and *Peter A. Burrough,* Using Public Domain Geostatistical and GIS Software for Spatial Interpolation.

Howard Veregin, Error Propagation through the Buffer Operation for Probability Surfaces.

Jim Vrabel, Multispectral Imagery Band Sharpening Study.

Jianjun Wang, Gary J. Robinson, and *Kevin White,* A Fast Solution to Local Viewshed Computation Using Grid-Based Digital Elevation Models.

David A. Yocky, Multiresolution Wavelet Decomposition Image Merger of Landsat Thematic Mapper and SPOT Panchromatic Data.

Ding Yuan, Natural Constraints for Inverse Area Estimate Corrections.